Geomechanics and Engineering, *Vol. 24, No. 1 (2021) 15-28*
DOI: https://doi.org/10.12989/gae.2021.24.1.015

Study on lateral behavior of digging well foundation with consideration of soil-foundation interaction

Yi Wang, Xingchong Chen, Xiyin Zhang*, Mingbo Ding, Jinhua Lu, and Huajun Ma

School of Civil Engineering, Lanzhou Jiaotong University, Lanzhou, 730070, China

(Received July 9, 2020, Revised December 15, 2020, Accepted December 20, 2020)

Abstract. Digging well foundation has been widely used in railway bridges due to its good economy and reliability. In other instances, bridges with digging well foundation still have damage risks during earthquakes. However, there is still a lack of knowledge of lateral behavior of digging well foundation considering the soil-foundation interaction. In this study, scaled models of bridge pier-digging well foundation system are constructed for quasi-static test to investigate their lateral behaviors. The failure mechanism and responses of the soil-foundation-pier interaction system are analyzed. The testing results indicate that the digging foundations tend to rotate as a rigid body under cyclic lateral load. Moreover, the depth-width ratio of digging well foundation has a significant influence on the failure mode of the interaction system, especially on the distribution of foundation displacement and the failure of pier. The energy dissipation capacity of the interaction system is discussed by using index of the equivalent viscous damping ratio. The damping varies with the depth-width ratio changing. The equivalent stiffness of soil-digging well foundation-pier interaction system decreases with the increase of loading displacement in a nonlinear manner. The absolute values of the interaction system stiffness are significantly influenced by the depth-width ratio of the foundation.

Keywords: railway bridge; digging well foundation; lateral behavior; soil-foundation interaction; quasi-static test

1. Introduction

In recent years, digging well foundation has been widely used in railway bridges due to its good economy, reliability and high integrity (Li 1997). For example, more than 300 digging well foundations have been applied in the Baoji-Zhongwei railway bridges and up to 31% of the foundations consists of digging well foundation in a viaduct of Qingdao-Haiyang intercity railway in China. Digging well foundation is particularly suitable for areas with small depth of bearing stratum. Fig. 1 shows the construction of digging well foundation used in Hangzhou-Shaoxing-Taizhou (HST) high-speed railway bridge in China.

As a kind of rigid foundation, the digging well foundation has better statics performance, but bridges with digging well foundation still has damage risk during earthquakes as it has been demonstrated by damages of bridges in earthquakes, such as Loma Prieta (USA) 1989, Kobe (Japan) 1995, Nepal 2015 (in Nepal and India)(Chowdhury *et al.* 2017). Figs. 2(a) and 2(b) show the falling beam of Chang-Qing Bridge due to the large displacement of digging well foundation and the damaged pier of Xin-Yi Bridge with digging well foundation during Ji-Ji earthquake in Taiwan, respectively.

In the past decades, researches on seismic performance of bridge foundations have been mainly focused on pile foundation(Wang *et al.* 2019, Chen *et al.* 2020, Liang *et al.* 2017, Zhang *et al.* 2020). However, the interaction of soil-rigid foundation-pier under seismic action is different from that of pile foundation due to the difference in mass and stiffness (Gaudio and Rampello 2020). Inertial actions cannot be neglected for rigid foundations, although that is frequently done for pile foundations. Previous researches on rigid foundation were mainly concentrated in the mechanical properties (Alampalli and Peddibotla 1997, Derakhshani 2017, Lai *et al.* 2020), bearing capacity (Karapiperis and Gerolymos 2014, Smith-Pardo *et al.* 2014, Conti, 2018, Pham *et al.* 2019, Sethy *et al.* 2020) and dynamic characteristics (Senjuntichai *et al.* 2006, Zheng *et al.* 2019). While few researches referred to the interaction of soil-rigid foundation-pier under seismic action. Zhu and Lee (2018) studied the interaction of soil-rigid foundation-structure in elastic homogenous half-space soil on analytical method and an analytic solution was presented. Han *et al.* (2019) investigated three-dimensional dynamic soil-structure interaction on cylindrical rigid foundation embedded in layered, fluid-saturated, poroelastic half-space using the indirect boundary element method. It was found that the pore fluid can affect the structural displacements significantly. Material and geometric nonlinearities between soil and foundation under seismic action have significant influence on the lateral bearing capacity of rigid foundation (Chiou *et al.* 2012). The static interaction between an eccentricly loaded rectangular rigid foundation and layered transversely isotropic soils is investigated and a solution of the layered transversely isotropic soils is derived using the analytical layer element method (Ai *et al.* 2020). However, the nonlinearity of the soil was not considered in these studies due to the limitation of research methods. At present, numerical simulation method is always used for seismic analysis of rigid foundation. Karapiperis and

*Corresponding author, Associate Professor, Ph.D.
E-mail: zhangxiyin@mail.lzjtu.cn

ISSN: 2005-307X (Print), 2092-6219 (Online)

Fig. 1 Digging well foundation of HST high-speed railway bridge

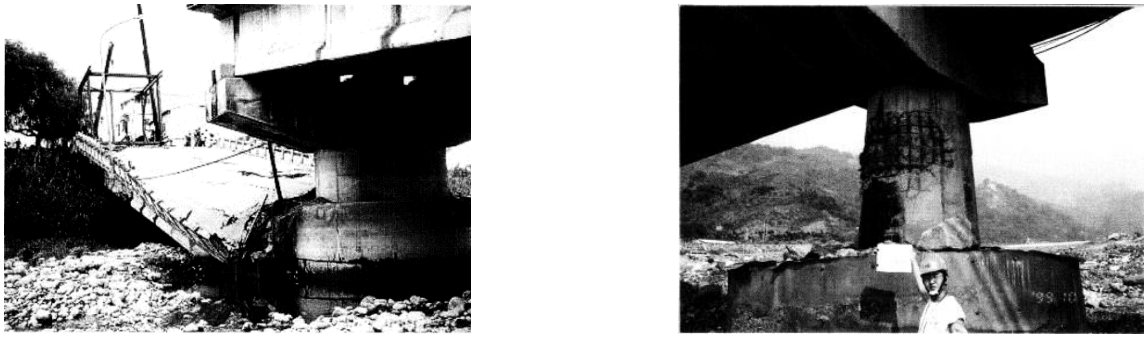

(a) Beam falling of the Xin-Yi Bridge (b) Pier damage of the Chang-Qing Bridge

Fig. 2 Destruction of bridges with digging well foundations in the Ji-Ji Earthquake

Gerolymos (2014) developed a seismic design procedure for caisson foundation supporting bridge piers by means of finite element analysis in 3D. Conti *et al.* (2020) studied the effect of caisson arrangement on seismic response of piers by finite element method. Gaudio and Rampello (2019) investigated the role of soil plasticity on the seismic performance of bridge piers founded on cylindrical caissons through a numerical study. Certainly, experimental method is also essential for analysis of the soil-rigid foundation-pier interaction, especially for its failure mechanism during larger lateral displacement under earthquake.

Existing researches are mainly aimed at developing simplified analytical methods of soil-rigid foundation-pier interaction and the whole interaction system is always simplified as a single degree of freedom system. This simplification is not conducive to analyze the failure mechanism of the soil-rigid foundation-pier system. Otherwise, the design method of the rigid foundation in current Chinese seismic design codes (Code for seismic design of railway engineering, 2009) is of linear elasticity and small deformation. This cannot meet the requirements for nonlinearity and large deformation of digging well foundation during earthquake. Therefore, it is essential to investigate the nonlinearity and failure characteristics of soil-digging well foundation-bridge pier system by experimental method.

In this paper, reduced scale models of the soil-digging well foundation-bridge pier interaction system are designed and quasi-static tests on scaled models are conducted to investigate their failure modes and nonlinearity behavior. The damage phenomenon, displacement distributions along the embedded depth, and the hysteretic behaviors of the models are discussed. Energy dissipation of the models is evaluated and stiffness degradation is analyzed. The results provide important references for the establishment of numerical model, and the evaluation of seismic performance of soil-digging well foundation-bridge pier interaction system.

Table 1 Similarity relation

Parameter	Symbol of similarity coefficient	Calculating formula	Similarity constant
Length	S_L	S_L	1/8
Strain	S_σ	S_σ	1
Stress	1	S_σ / S_E	1
Modulus of elasticity	S_E	$S_E = S_\sigma$	1
Area	S_A	S_L^2	1/64
Moment of inertia	S_I	S_L^4	1/4096
Vertical force	S_F	$S_\sigma S_L^2$	1/64

2. Experimental design

2.1 Model design

In these experiments, a bridge pier with digging well foundation from a railway bridge in China is selected as the prototype. Two 1/8 reduced-scale models are designed and fabricated for quasi-static test based on the prototype bridge, where the cross section of the foundations is rectangular. Detailed scaling similarities based on a generalized Π theorem are shown in Table 1 (Soninl *et al.* 2004). The external force acted on the scaled model is $1/L^2$

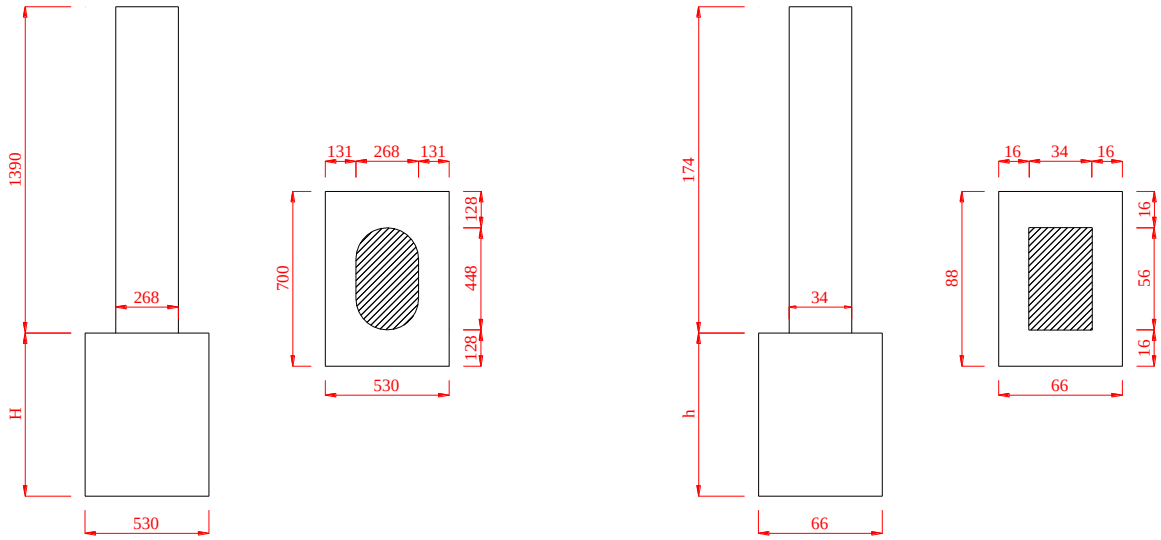

(a) Prototype structure(H=350,700) (b) Scaled model(h=44,88)

Fig. 3 Size of the bridge pier with pile foundation (unit: cm)

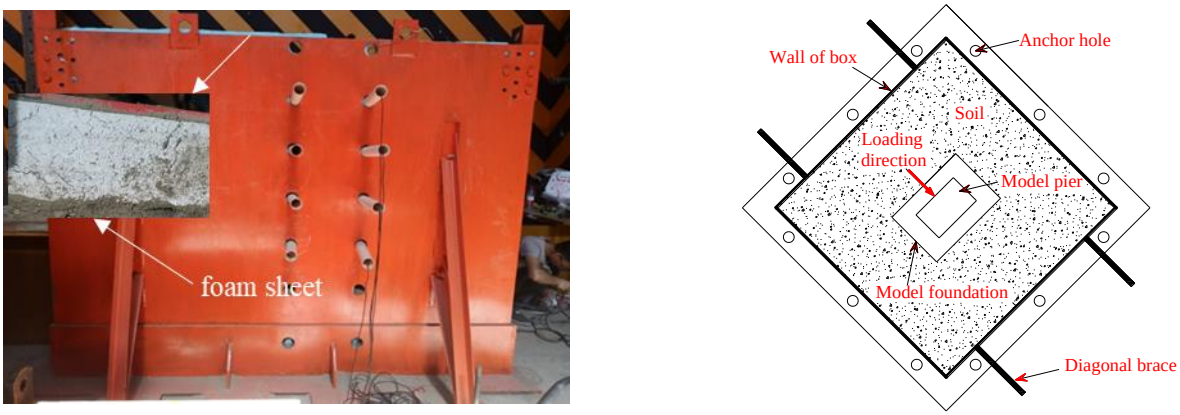

(a) Steel soil container (b) Plan view of the soil container

Fig. 4 Details of the soil container

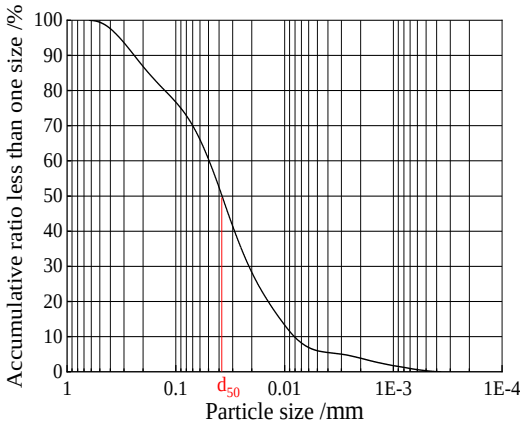

Fig. 5 Soil particle distribution

times of the prototype and the lateral displacement is 1/L times of the prototype according to the similarity relations. The round-ended pier in the prototype is simplified to the rectangular section according to the similarity of moment of inertia in the scale model for simplifying construction. It should be noted that the insufficient mass density of soil can be made up by tamping soil as much as possible (Zhang *et al.* 2020). The sizes of the prototype and scaled model pier with digging well foundation are shown in Figs. 3(a) and 3(b), respectively. They have different depth-to-width ratios of foundation and are labeled as D-1 (1.33 depth-to-width ratio) and D-2 (0.67 depth-to-width ratio), respectively. The

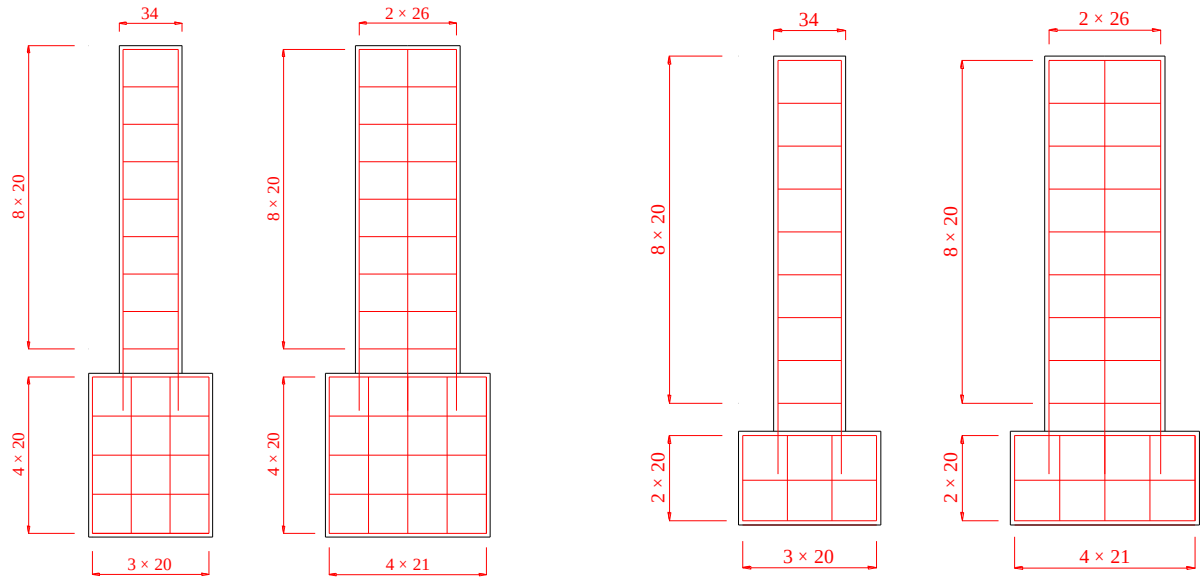

(a) D-1 (b) D-2

Fig. 6 Reinforcement arrangement of the model pier

(a) Steel cage banding (b) Foundation pit excavating (c) Concrete pouring (d) Concrete curing

Fig. 7 Model making process

size (length, width and height) of model pier is 56 cm×34 cm×174 cm, transverse reinforcement of which is 8 mm in diameter with the equal spacing of 200 mm. Six longitudinal steel bars with a diameter of 12 mm are used in model pier, which constitute a 0.38% steel ratio. The railway bridge piers have low reinforcement ratio (less than 0.5%) in China (Lu *et al.* 2019). A certain amount of constructional reinforcement with a diameter of 12 mm is arranged in the digging well foundation according to the seismic design specification (Code for seismic design of railway engineering 2009).

2.2 Soil container and material parameters

For the implementation of the experiment, a rigid square steel container with a size of 250 cm×250 cm×200 cm (length × width × height) and wall thickness of 1 cm is processed to constrain the soil, where the 8 cm thick foam sheets are used to reduce the boundary effect of the container, as shown in Figs. 4(a). The bottom of the container is welded to a base plate with a size of 280 cm×280 cm×1 cm. The plate is then fixed to the laboratory floor by 12 screws with a diameter of 80 mm. To increase the stability of the soil container, four diagonal braces are added in the loading direction. Plan view of the soil container is shown in Fig. 4(b).

The soil used in the experiments is selected from Northwest China, where several high-speed railways have been constructed. The soil gradation curve is measured and plotted in Fig. 5. According to the standards for classification of soils (Code for rock and soil classification of railway Engineering 2019), it is classified as the silt. The water content of the soil is 14.2%, which is determined by the moisture content test. Bulk density is 1.8 $g \cdot cm^{-3}$ determined by the density test.

The cube compressive strength of the concrete used in the experiments is 30.2 MPa which is measured after curing until the 28th day. It has an elastic modulus of 2.0×10^4 MPa. The standard yield strength of steel reinforcing bars used in the model pier are 335 MPa. The reinforcement

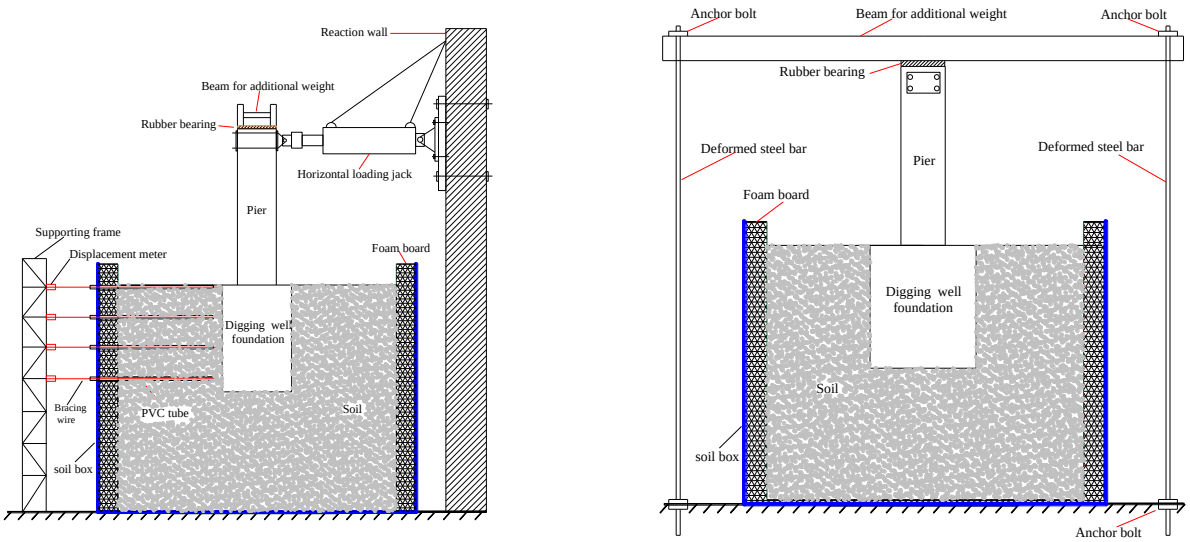

(a) Lateral loading unit (b) Vertical loading unit

Fig. 8 Loading system for quasi-static testing

Fig. 9 Layout of the loading system

arrangement of the models is shown in Fig. 6.

2.3 Model fabrication

Model making includes the following processes, as shown in Fig. 7.

First is steel cage banding; then are foundation pit excavating and concrete pouring; and finally, the concrete is cured.

(a) Steel cage banding: Before casting of models, the steel cages of the pier and foundation are assembled using longitudinal bars and stirrups.

(b) Foundation pit excavating: The soil is first wetted (about 14.2% water content) and then kept for 24 hours to make the moisture content distribute uniformly. The soil is packed into the container in layers (20 cm per layer) and compacted by electric compactor. The foundation pit is excavated manually after the soil is rammed to the design height.

(c) Concrete pouring: After excavation of the foundation pit, the steel cages of the foundation are installed in the foundation pit, and then foundation concrete is poured and vibrated manually.

(d) Concrete curing: The concrete is cured for 28 days until it reaches the designed strength.

2.4 Test apparatus

The tests are conducted at the structural laboratory of Lanzhou Jiaotong University. The experimental devices consist of soil container, loading system and data acquisition system. The loading system is composed of horizontal loading unit and vertical loading unit. The lateral loading unit is equipped by an electro-hydraulic servo loading system, and it is horizontally connected to the pier head, as shown in Fig. 8(a). An H-shaped steel beam and two high-strength deformed bars with anchor bolts form the vertical loading unit, it can be loaded by tightening the bolt, as shown in Fig. 8(b). The loading system layout is illustrated in Fig. 9.

2.5 Measuring point arrangement

During testing, the pier-top displacement is obtained by the lateral loading unit. The lateral displacement of the foundation is measured along its depth at the loading direction by displacement meters, as shown in Fig. 10. First, when the soil is filled at the height of measuring points, the

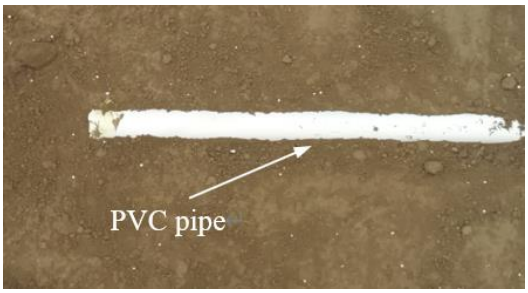

(a) PVC pipe

(b) Test points

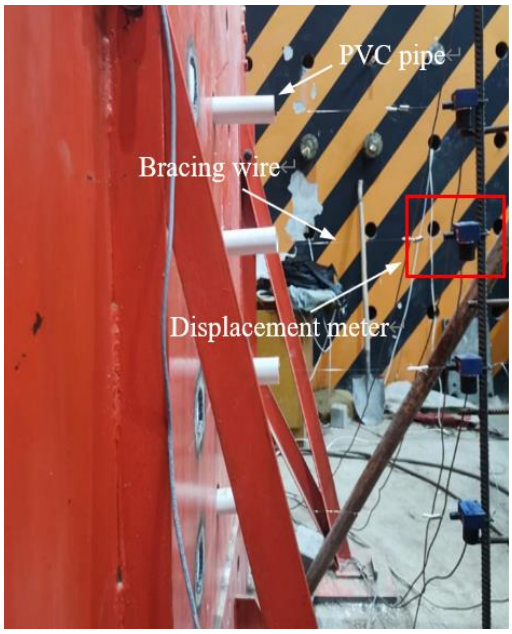

(c) Displacement transducers

Fig. 10 Measurement method of lateral displacement for foundation

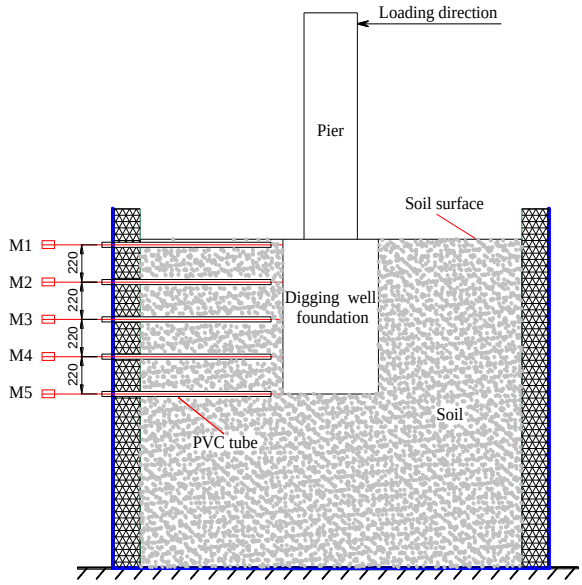

(a) D-1

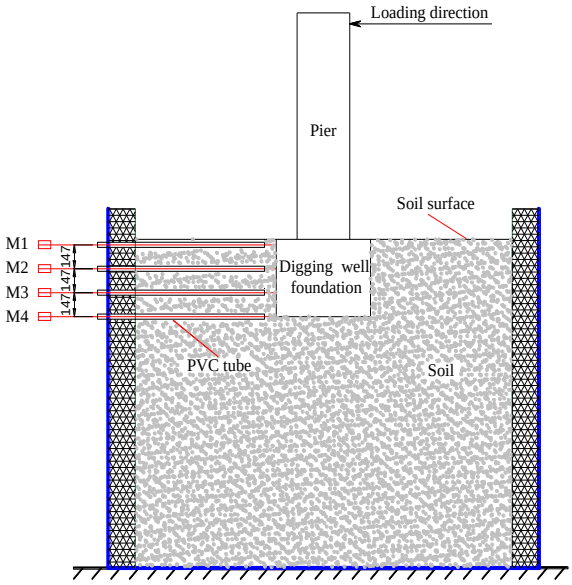

(b) D-2

Fig. 11 Layout of the displacement measuring point

PVC pipe is buried at the level of the measuring point to protect the wires (Fig. 10(a)). After excavation of the foundation pit, the bracing wire is passed through the PVC pipe and connected to displacement meters (Fig. 10(c)). Finally, the other end of the bracing wire is connected to the measuring point located on the digging well foundation (Fig. 10(b)). It should be noted that the bracing wire is specially treated at the measuring point to ensure that it is as close to the center of the PVC pipe as possible (Fig. 10(b)). Displacement meters are installed to measure the displacement of the foundation along the depth. They are numbered as M1-M5 with an equal spacing of 220 mm in model D-1 and as M1-M4 with an equal spacing of 147 mm in model D-2, as shown in Fig. 11(a) and 11(b).

2.6 Loading scheme

The loading displacement is applied by the horizontal electro hydraulic servo jack, and it is controlled by the displacement-controlled paths. Loading scheme consists of two different phases: (1) the first phase includes 2 mm, 4 mm, 6 mm, 8 mm, 10 mm, 12 mm, and 15 mm; (2) the second phase is 15 mm to 50 mm with increment of 5 mm; each loading grade repeats 3 times. The loading displacement history is shown in Fig. 12. A constant load (57 kN) in vertical direction is applied at the top of bridge

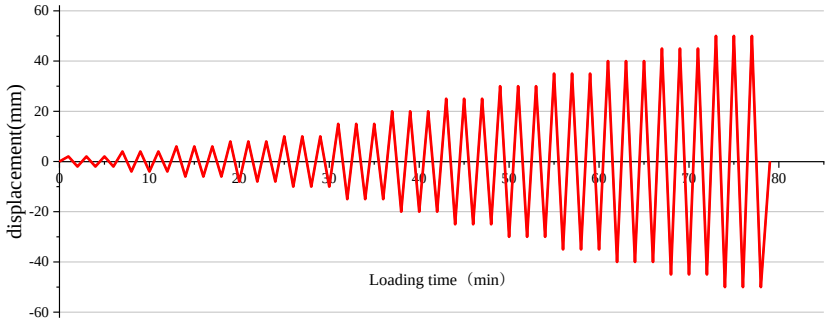

Fig. 12 Displacement history with displacement control method

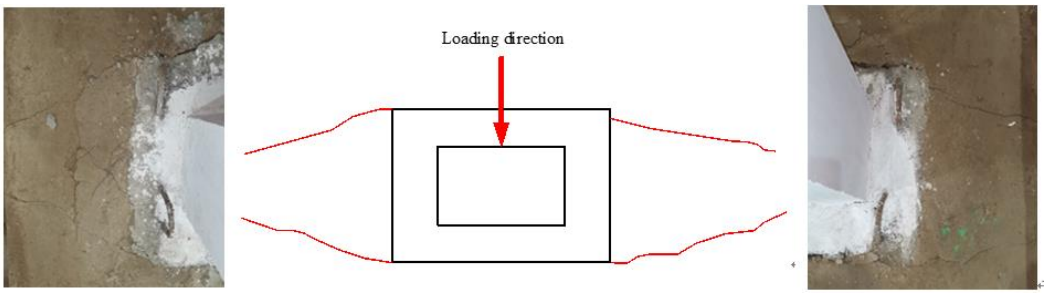

Fig. 13 Crack distributions at soil surface after testing

(a) Foundation of D-1 (b) Lateral crack of D-1

Fig. 14 Failure phenomenon of the D-1 foundation after testing

pier by tightening anchor bolts as a consideration of the weight of the superstructure, which is the sum of the weight of the superstructure and accessory structure. It is obtained after scaling (1/64).

3. Experimental results

3.1 Failure characteristics

Two models of piers supported by digging well foundations in silt are studied under horizontal reciprocating loading, and their failure characteristics are observed. When the loading displacement of the model D-1 and D-2 reaches 6 mm and 4 mm respectively, slight separation appears between the foundation and surrounding soil at the soil surface. When the loading displacement of the model D-1 and D-2 reaches 8 mm and 6 mm respectively, the first micro soil crack appears on the side of the foundation. Subsequently, with the increasing of loading displacement, the cracks continue to expand and their width and depth increase. After testing, four main soil cracks are observed. The direction trend of soil cracks closes to the foundation is approximately perpendicular to the loading direction. Away from the foundation, the two cracks at the same side gradually converge towards to center, as shown in Fig. 13 (taking the model D-2 for example).

After testing, the foundation of the two models is excavated to observe their damages, as shown in Figs.14(a) and 14(b) for D-1 and in Figs. 15(a)-15(d) for D-2. As seen in Figs.14 and 15, the foundations have no damage, but they are separated from the side soil and uplifted at the base. In addition, the lateral separation and base uplift of the model D-2 is about 8 mm and 4 mm respectively (Fig. 15(c)), while that of the model D-1 is about 4 mm and 1 mm. This indicates that the damage of the soil around D-2 is more severely than that around D-1.

No cracks are observed in the pier of the model D-2,

(a) Foundation of D-2 (b) Lateral crack of D-2 (c) Cracks in detail (d) Bottom crack of D-2

Fig. 15 Failure phenomenon of the D-2 foundation after testing

Fig. 16 Comparison of the failure phenomena for the two model piers after testing

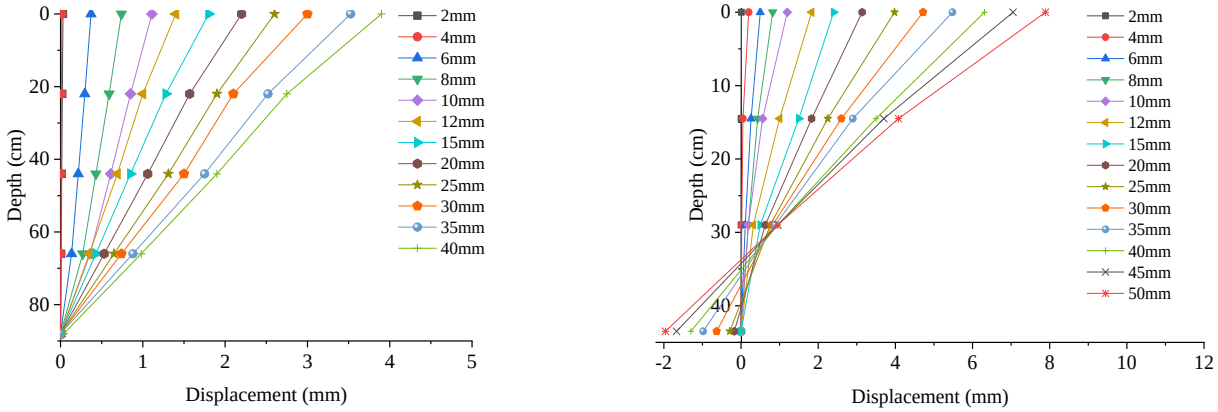

(a) D-1 (b) D-2

Fig. 17 Displacement distributions of the foundations under different loading displacement

while concrete cracking and steel bars yielding occur at the bottom of the pier for the model D-1, as shown in Fig.16. This indicates the pier of the model D-2 is mainly in elastic state while that of the D-1 is in nonlinear state under cyclic loading. Because the mobilisation degree of shear strength of soil in model D-2 are fully developed compared with that of model D-1, then model D-2 produces more significant rigid body rotation than model D-1 under cyclic lateral loads (Zafeirakos and Gerolymos 2013, Gaudio and Rampello 2020).

3.2 Displacement distribution of the foundation

Fig. 17(a) and 17(b) show the lateral displacement distributions along the foundation depth for D-1 and D-2 respectively, zero position is the bottom of the pier and downward is the positive. It can be seen from the figures that the main deformation of the two foundations is the rigid body rotation. After testing, the displacement of the D-2 foundation at the top reaches 8.1 mm while that of the D-1 foundation is 3.9 mm. In addition, the foundation D-2

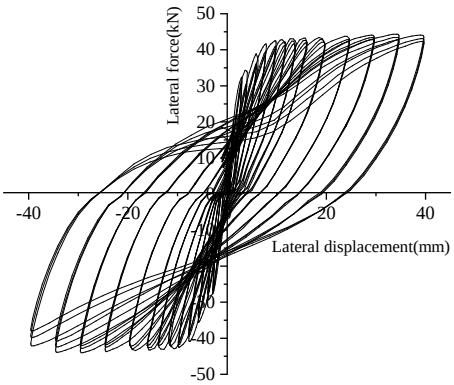

(a) D-1

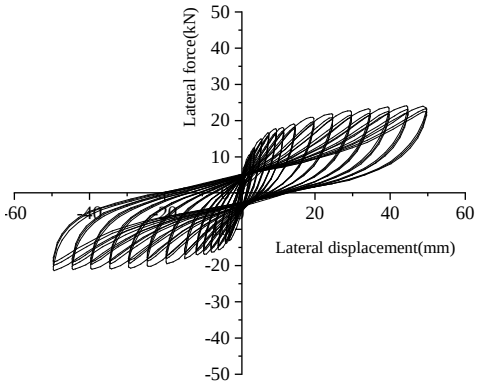

(b) D-2

Fig. 18 Hysteretic curves of the models

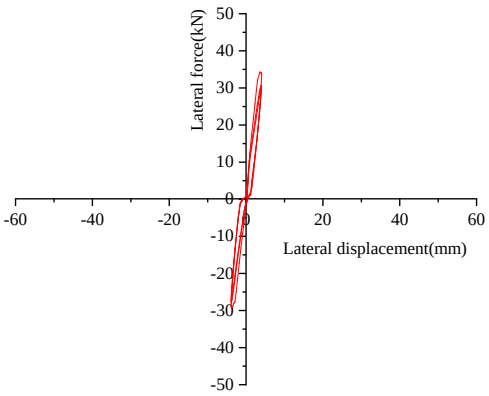

(a) 4 mm loading displacement (D-1)

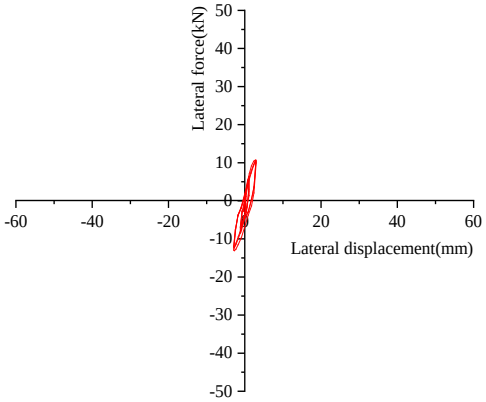

(b) 4 mm loading displacement (D-2)

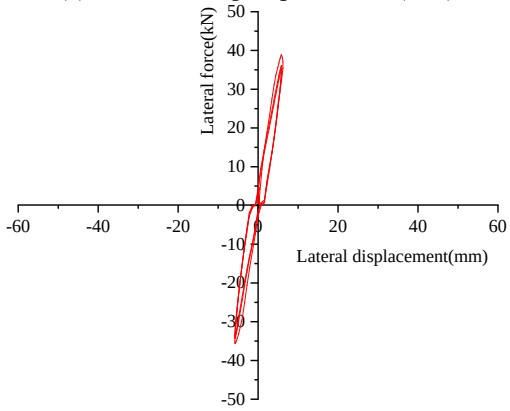

(c) 6 mm loading displacement (D-1)

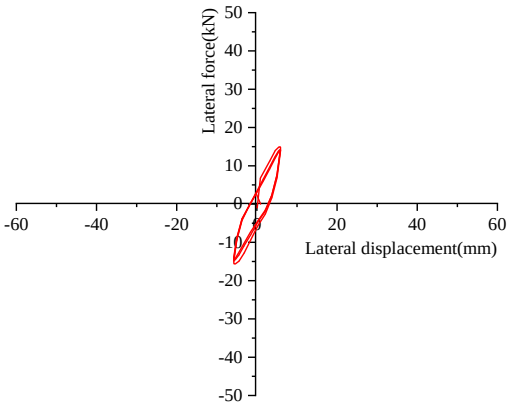

(d) 6 mm loading displacement (D-2)

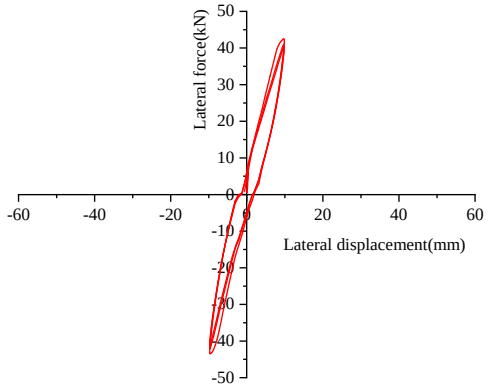

(e) 10 mm loading displacement (D-1)

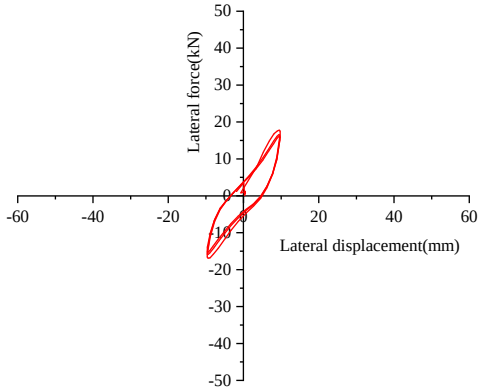

(f) 10 mm loading displacement (D-2)

Fig. 19 Hysteretic hoops under critical loading steps

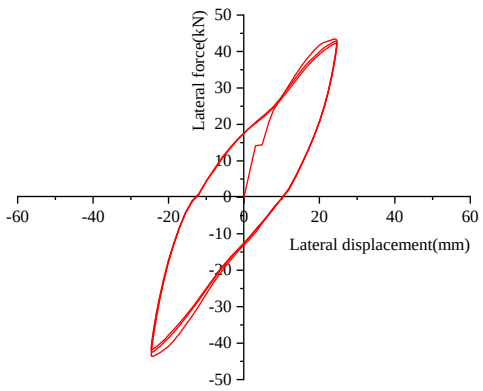

(g) 25 mm loading displacement (D-1)

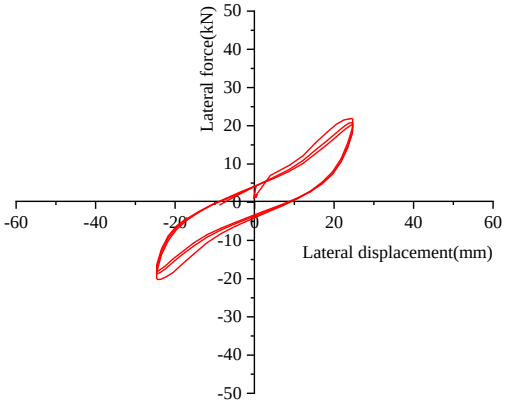

(h) 25 mm loading displacement (D-2)

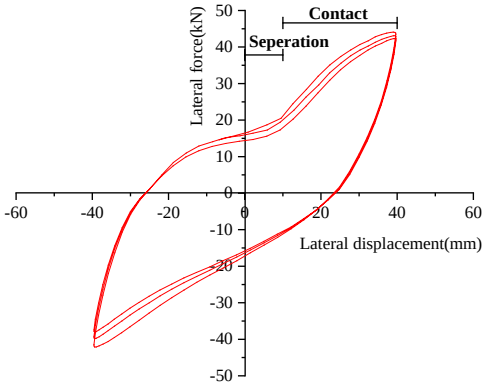

(i) 40 mm loading displacement (D-1)

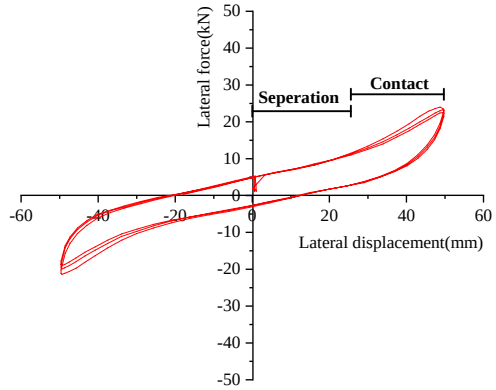

(j) 50 mm loading displacement (D-2)

Fig. 19 Continued

experiences negative displacement at the larger embedded depth and reaches the maximum of -1.9 mm at the bottom after the 20 mm loading displacement due to the yielding of soil at the top layers. Interestingly, the rotation center of the foundation D-1 is always at the bottom of the foundation. But the rotation center of the foundation D-2 moves upward from the bottom of the foundation to about 2/3h of embedded depth with increasing of loading displacement, it is mainly caused by the yielding of soil at the bottom of the foundation D-2.

4. Results analysis

4.1 Hysteretic behaviors

The relationships between the pier-top lateral force and displacement (hysteretic curve) are plotted as shown in Fig.18a–b for D-1 to D-2, respectively. To analyze the force-displacement development rule of the models, the hysteretic hoops for D-1 and D-2 under critical loading steps are extracted and plotted separately, as shown in Figs. 19(a)-19(j). It can be found that at the initial loading stage, the load increases linearly with the displacement, indicating that the soil-foundation-pier system keeps elastic. With increasing of loading displacement, the areas of hysteretic loops become larger, which suggests the energy dissipation capacity increases and the soil-foundation-pier interaction becomes stronger. The hysteretic hoops become pinched shape at larger loading displacement. This is attributed to the reasons: separation and uplift between foundation and soil occur. Before foundation contacting with the soil, the stiffness of soil-foundation-pier system is small. Subsequently, the stiffness of the system increases rapidly as seen in Fig. 19(i) and 19(j). From the shape of the hysteretic loop, D-1 has a better energy dissipation capacity than D-2 due to its plumped hysteretic loop.

4.2 Skeleton curves

Based on the hysteretic curves, the skeleton curves of the two models are plotted in Fig. 20. Table 2 presents the elastic critical load f_{cr}, the ultimate load f_m, the elastic critical deformation y_{cr} and the maximum deformation y_m of D-1 and D-2, respectively. It can be found that the skeleton curves of both models are antisymmetric. For example, the positive ultimate elastic displacement and load of D-1 are 4.0 mm and 34.4 kN, respectively, while the negative ultimate elastic displacement and load are −3.9 mm and −34.1 kN, respectively, as shown in Fig. 20a. The positive ultimate displacement and load of D-1 are 35.0 mm and 44.3 kN, respectively, while the negative ultimate displacement and load of D-1 are −35.2 mm and −43.9 kN, respectively. In addition, the ultimate load of D-1 is 83.1% larger than that of D-2, while the ultimate displacement is 30% smaller. The bearing capacity and displacement ductility of the soil-foundation-pier system are greatly affected by the depth-to-width ratio of foundation.

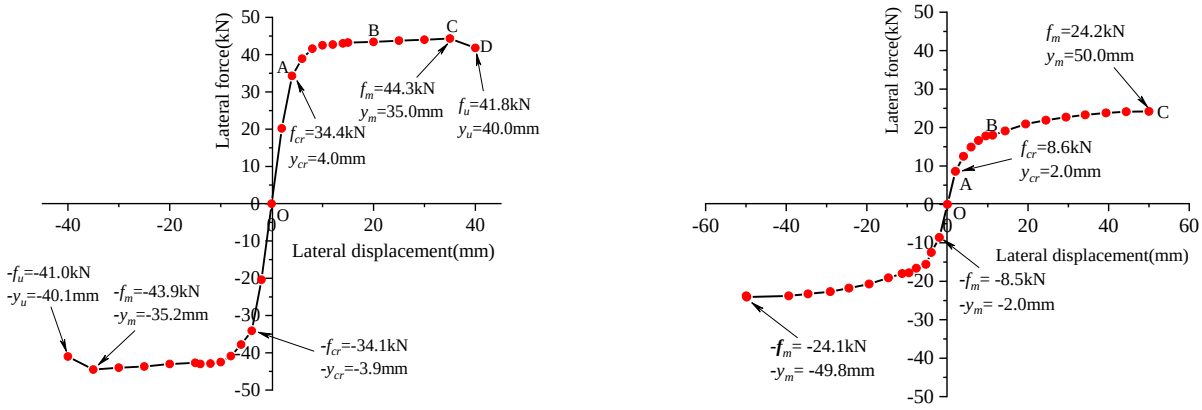

(a) D-1 (b) D-2

Fig. 20 Skeleton curves of the models

Table 2 The elastic critical and ultimate values of the two models

Model	f_{cr}/ kN	y_{cr}/ mm	f_m/ kN	y_m/ mm	f_u/ kN	y_u/ mm
D-1	34.4	4.0	44.3	35.0	40.0	41.8
D-2	8.6	2.0	24.2	50.0	-	-

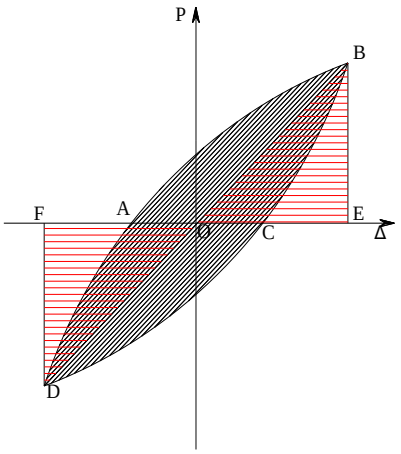

Fig. 21 Typical hysteretic loop

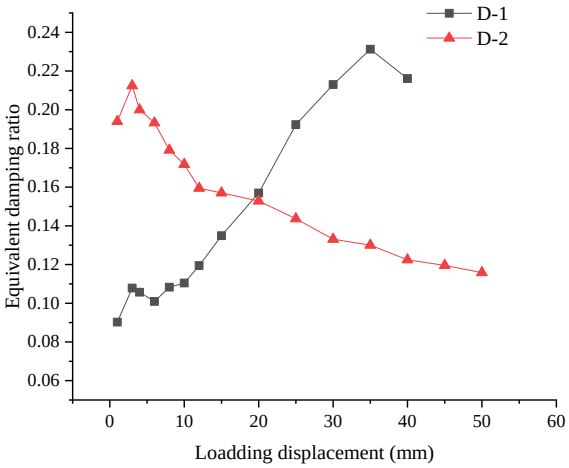

Fig. 22 Equivalent damping ratio of the two models

As seen in Fig. 20, the skeleton curves can be divided into four stages, namely, the elastic stage (O-A), the elastic-plastic stage (A-B), the plastic hardening stage (B-C) and the failure stage (C-D). In the elastic stage, the load increases linearly with the displacement. The end point of the elastic phase is marked as 'A' with the displacement y_{cr}. Point 'A' represents that the soil begins to crack and the stiffness of the system starts to decrease.

During the elastic-plastic stage (A-B) of D-1, the stiffness of the model decreases gradually due to the cracking of foundation soil and pier concrete. The skeleton curve of D-1 has obvious yield range extended from 10 mm to 20 mm, it shows that D-1 has better plastic property. However, there is no yield range in the skeleton curve of D-2. This is mainly attributed to the fact that the pier concrete of D-2 has no cracks, which also leads to the stiffness degradation of D-2 mainly due to the soil cracking.

In the plastic hardening stage (B-C), the lateral load of the model increases slowly while the displacement increases rapidly. When the skeleton curve reaches point 'C', the bearing capacity of the model reaches its peak. That means the bearing capacity of the soil-digging well foundation-bridge pier interaction system no longer increases due to the severe damage of the soil and pier concrete. It is worth noting that the bearing capacity of the D-2 is about half that of the D-1, that is because the bearing capacity of the system is not fully exerted due to the small foundation depth-to-width ratio of D-2.

During the failure stage (C-D) of D-1, the lateral load of the model decreases with the increase of displacement. The model D-1 is destroyed when the skeleton curve reaches point 'D'. Since the pier concrete of model D-2 is always in an elastic state and the soil used in the tests is silt, the skeleton curve of model D-2 has no failure stage (C-D) compared with model D-1.

4.3 Equivalent viscous damping

The equivalent damping ratio ξ_{eq} is an important index

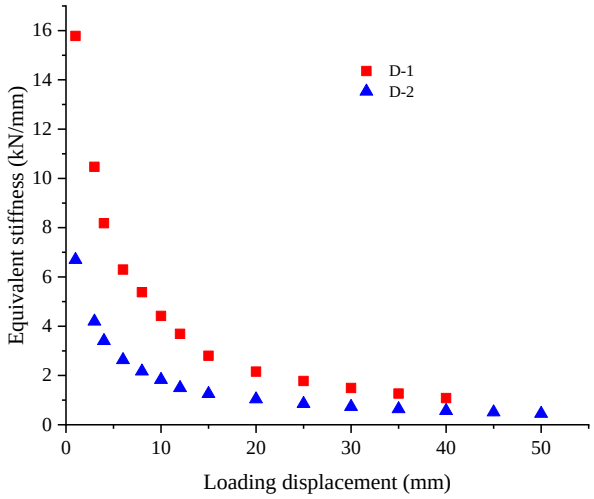

Fig. 23 Equivalent stiffness of the models

to evaluate the energy dissipation capacity of a bridge and can be calculated by Eq. (1) (Zheng *et al.* 2020).

$$\xi_{eq} = \frac{1}{2\pi} \frac{S_{ABCD}}{S_{OFD} + S_{OBE}} \tag{1}$$

As seen in Fig. 21, S_{ABCD} is the area of the hysteresis loop; S_{OFD}+ S_{OBE} represents the elastic strain energy stored in the system. Based on Eq. (1), the equivalent viscous damping ratios of the two models under different loading displacement are calculated and plotted in Fig. 22.

From Fig. 22, the damping ratios of the models vary between 9% and 23%, and their average is 15.5%. The models possess high energy dissipation capacity, which is implied by the average damping ratio of 15.5%.

At the initial loading stage, the equivalent damping ratio of model D-1 increases first with the loading displacement, and then decreases due to the failure of foundation soil. With the continuing of loading, the equivalent damping ratio increases again to the maximum and then decreases. This is owing to the cracking of the bridge pier and the yield of the steel bars, which leads to the increasing of energy dissipation capacity for the model D-1. Subsequently, the equivalent damping ratio decreases again due to the yield of the reinforcement and the failure of the bridge pier.

The equivalent damping ratio of model D-2 shows an overall downward trend. Because the pier is not damaged after the foundation soil yields, and all the energy consumption of the system comes from the soil.

4.4 Equivalent stiffness

Secant stiffness is often used as equivalent stiffness to study the stiffness degradation. It reflects the seismic performance of a system and can be calculated by Eq. (2) based on the experimental specification of earthquake engineering (Specificating of testing methods of earthquake resistant building 1996).

$$K_i = \frac{|+F_i| + |-F_i|}{|+\Delta_i| + |-\Delta_i|} \tag{2}$$

where, $+F_i$ and $-F_i$ represent the maximum positive and negative transverse loads at different loading stages. $+\Delta_i$ and $-\Delta_i$ are maximum positive and negative displacements corresponding to the maximum positive ($+F_i$) and negative ($-F_i$) transverse loads, respectively. The equivalent stiffness of the models at different loading stages is calculated and plotted in Fig. 23. As seen from the diagram, the equivalent stiffness decreases with the increase of loading displacement in a nonlinear manner. The equivalent stiffness of model D-1 decreased from the initial 15.78 kN/mm to the final 1.08 kN/mm, while that of Model D-2 decreased from 6.7 kN/mm to 0.45 kN/mm. In addition, although the pier is not damaged, the equivalent stiffness of the model D-2 is smaller than that of the model D-1. This suggests that the depth-to-width ratio of foundation has an important effect on the absolute values of system stiffness.

5. Conclusions

In this study, quasi-static tests of two 1/8 scaled models are carried out to investigate the seismic behavior of bridge pier on digging well foundation with different depth-to-width ratios. The failure phenomenon, displacement distributions, hysteretic curves, skeleton curves, stiffness degradation and the damping ratios of the soil-foundation-pier interaction system are discussed. Some primary conclusions are drawn as follows.

• Soil cracks occur at the two foundations. Model D-1 with larger depth-to-width ratio suffer concrete cracking and steel yielding at the bottom of the pier. While the pier of model D-2 with lower depth-to-width ratio has no damage. From the displacement distribution, the two foundations tend to rotate as a rigid body under cyclic lateral load. The rotation center of D-1 is always at the bottom of the foundation, while the rotation center of D-2 moves upward with the increase of loading displacement, which indicates the depth-to-width ratio of foundation has an important effect on the soil-foundation interaction.

• The hysteretic behavior shows that model D-1 has better energy dissipation capacity than model D-2, because the large depth-to-width ratio of foundation can bring out potential energy dissipation capacity of the pier. Based on the skeleton curve, the soil-digging well foundation-pier system experience four stages under lateral loading i.e. elastic stage, elastic-plastic stage, plastic-hardening state and failure stage. It is worth noting that the skeleton curve of model D-2 has no failure stage compared with model D-1, which is mainly because the pier concrete of model D-2 is always in an elastic state and the soil used in the tests is silt.

• The equivalent damping ratio of model D-1 tends to rise first and then fall, while that of model D-2 tends to fall. The reason is that all the energy consumption of the model D-2 comes from the soil while that of the model D-1 comes from the soil and pier.

• The equivalent stiffness of soil-digging well foundation-pier interaction system decreases with the increase of loading displacement in a nonlinear manner. Although the pier is not damaged, the equivalent stiffness of the model D-2 is smaller than that of the model D-1. The

absolute values of the interaction system stiffness are significantly influenced by the depth-width ratio of the foundation.

Acknowledgments

This research is supported by the National Natural Science Foundation of China (Grants No. 51968039, 51768036, 51808273), China Postdoctoral Science Foundation (Grant No. 2018M643767), Youth Talent Support Project of China Association for Science and Technology (for Xiyin Zhang), Science and Technology Program of Gansu Province for Distinguished Young Scholars (No. 20JR5RA430), Tianyou Youth Talent Lift Program of Lanzhou Jiaotong University (Xiyin Zhang), and lzjtu (201801) EP support. On behalf of all authors, the corresponding author states that there is no conflict of interest.

References

Ai, Z. and Jiang, Y. (2020), "Dual integral equation solution of eccentricly loaded rectangular rigid foundation embedded in layered transversely isotropic soils", *Comput. Geotech.*, **126**, 1-22. https://doi.org/10.1016/j.compgeo.2020.103755.

Alampalli, S. and Peddibotla, V. (1997), "Laboratory investigation on Caissons-deformations and vertical load distributions", *Soils Found.*, **37**(2), 61-69. https://doi.org/10.3208/sandf.37.2_61.

Chen, X., Zhang, X., Zhang, Y., Mingbo, D. and Yi, W. (2020), "Hysteretic behaviors of pile foundation for railway bridges in loess", *Geomech. Eng.*, **20**(4), 323-331. https://doi.org/10.12989/gae.2020.20.4.323.

Chiou, J.S., Ko, Y.Y., Hsu, S.Y. and Tsai, Y.C. (2012), "Testing and analysis of a laterally loaded bridge caisson foundation in gravel", *Soils Found.*, **52**(3), 562-573. https://doi.org/10.1016/j.sandf.2012.05.013.

Chowdhury, I., Tarafdar, R., Ghosh, A. and Dasgupta, S.P. (2017), "Dynamic soil structure interaction of bridge piers supported on well foundation", *Soil Dyn. Earthq. Eng.*, **97**, 251-265. https://doi.org/10.1016/j.soildyn.2017.03.005.

Conti, R. (2018), "Simplified formulas for the seismic bearing capacity of shallow strip foundations", *Soil Dyn. Earthq. Eng.*, **104**, 64-74. https://doi.org/10.1016/j.soildyn.2017.09.027.

Conti, R., Laora, R.D., Licata, V., Iovino, M. and Sanctis, L.D. (2020), "Seismic performance of bridge piers: Caisson vs pile foundations", *Soil Dyn. Earthq. Eng.*, **130**, 1-15. https://doi.org/10.1016/j.soildyn.2019.105985.

Derakhshani, A. (2017), "Estimating uplift capacity of suction caissons in soft clay: A hybrid computational approach based on model tree and GP", *Ocean Eng.*, **146**, 1-8. https://doi.org/10.1016/j.oceaneng.2017.09.025.

Gaudio, D. and Rampello, S. (2019), "The influence of soil plasticity on the seismic performance of bridge piers on caisson foundations", *Soil Dyn. Earthq. Eng.*, **118**, 120-133. https://doi.org/10.1016/j.soildyn.2018.12.007.

Gaudio, D. and Rampello, S. (2020), "Equivalent seismic coefficients for caisson foundations supporting bridge piers", *Soil Dyn. Earthq. Eng.*, **129**, 1-14. https://doi.org/10.1016/j.soildyn.2019.105955.

Gaudio, D. and Rampello, S. (2020b), "On the assessment of seismic performance of bridge piers on caisson foundations subjected to strong ground motions", *Earthq. Eng. Struct. Dyn.*, 1-22. https://doi.org/10.1002/eqe.3407.

GB 50111-2006 (2009), Code for seismic design of railway engineering. Ministry of Housing and Urban-Rural Development, Beijing, China.

Han, B., Liang, J., Fu, J. and Liu, R. (2019), "3D dynamic soil-structure interaction in layered, fluid-saturated, poroelastic half-space", *Soil Dyn. Earthq. Eng.*, **120**, 113-126. https://doi.org/10.1016/j.soildyn.2019.01.027.

JGJ101-96 (1996), Specificating of testing methods of earthquake resistant building, Ministry of Housing and Urban-Rural Development, Beijing, China.

Karapiperis, K. and Gerolymos, N. (2014), "Combined loading of caisson foundations in cohesive soil: Finite element versus Winkler modeling", *Comput. Geotech.*, **56**, 100-120. https://doi.org/10.1016/j.compgeo.2013.11.006.

Lai, F., Liu, S., Deng, Y., Sun, Y., Wu, K. and Liu, H. (2020), "Numerical investigations of the installation process of giant deep-buried circular open caissons in undrained clay", *Comput. Geotech.*, **118**, 1-17. https://doi.org/10.1016/j.compgeo.2019.103322.

Li, T. (1997), "Design method of dug well foundation of bridge in loess area", *Chin. J. Geotech. Eng.*, **19**(3), 47-54.

Liang, F., Jia, Y., Sun, L., Xie, W. and Chen, H. (2017), "Seismic response of pile groups supporting long-span cable-stayed bridge subjected to multi-support excitations", *Soil Dyn. Earthq. Eng.*, **101**, 182-203. https://doi.org/10.1016/j.soildyn.2017.07.019.

Lu, J., Chen, X., Ding, M., Zhang, X., Liu, Z. and Yuan, H. (2019), "Experimental and numerical investigation of the seismic performance of railway piers with increasing longitudinal steel in plastic hinge area", *Earthq. Struct.*, **17**(6), 545-556. https://doi.org/10.12989/eas.2019.17.6.545.

Pham, Q.N., Ohtsuka, S., Isobe, K., Fukumoto, Y. and Hoshina, T. (2019), "Ultimate bearing capacity of rigid footing under eccentric vertical load", *Soils Found.*, **59**(6), 1980-1991. https://doi.org/10.1016/j.sandf.2019.09.004.

Senjuntichai, T., Mani, S. and Rajapakse, R.K.N.D. (2006), "Vertical vibration of an embedded rigid foundation in a poroelastic soil", *Soil Dyn. Earthq. Eng.*, **26**(6-7), 626-636. https://doi.org/10.1016/j.soildyn.2006.01.013.

Sethy, B.P., Patra, C.R., Das, B.M. and Sobhan, K. (2020), "Behavior of circular foundation on sand layer of limited thickness subjected to eccentrically inclined load", *Soils Found.*, **60**(1), 13-27. https://doi.org/10.1016/j.sandf.2019.12.005.

Smith-Pardo, J.P., Ortiz, A. and Blandon, C.A. (2014), "Biaxial capacity of rigid footings: Simple closed-form equations and experimental results", *Eng. Struct.*, **69**, 149-157. https://doi.org/10.1016/j.engstruct.2014.03.007.

Sonin, A.A. (2004), "A generalization of the Π-theorem and dimensional analysis", *Proc. Nat. Acad. Sci.*, **101**(23), 8525-8526. https://doi.org/10.1073/pnas.0402931101.

TB 10077-2019 (2019), Code for rock and soil classification of railway Engineering, State Railway Administration, Beijing, China.

Wang, X., Ye, A. and Ji, B. (2019), "Fragility-based sensitivity analysis on the seismic performance of pile-group-supported bridges in liquefiable ground undergoing scour potentials", *Eng. Struct.*, **198**, 1-15. https://doi.org/10.1016/j.engstruct.2019.109427.

Zafeirakos, A. and Gerolymos, N. (2013), "On the seismic response of under-designed caisson foundations", *B. Earthq. Eng.*, **11**(5), 1337-1372. https://doi.org/10.1007/s10518-013-9465-0.

Zhang, X., Chen, X., Wang Y., Ding, M., Lu, J. and Ma, H. (2020), "Quasi-static test of the precast-concrete pile foundation for railway bridge construction", *Adv. Concrete Construct.*, **10**(1), 49-59. https://doi.org/10.12989/acc.2020.10.1.049.

Zhang, Y., Chen, X., Zhang, X., Ding, M., Wang, Y. and Liu, Z.

(2019), "Nonlinear response of the pile group foundation for lateral loads using Pushover analysis", *Earthq*. *Struct*., **19**(4), 273-286. https://doi.org/10.12989/eas.2020.19.4.273.

Zheng, C., He, R., Kouretzis, G. and Ding, X. (2019), "Horizontal vibration of a cylindrical rigid foundation embedded in poroelastic half-space", *Comput*. *Geotech*., **106**, 296-303. https://doi.org/10.1016/j.compgeo.2018.11.009.

Zheng, L., Sandra, E., Wang, Y. and Panagiotis, K. (2020), "Study on the stiffness degradation and damping of pile foundations under dynamic loadings", *Eng*. *Struct*., **203**, 1-20. https://doi.org/10.1016/j.engstruct.2019.109850.

Zhu, G. and Lee, V.W. (2018), "Three-dimensional (3D) soil structure interaction with normal-plane P-wave incidence: Rigid foundation", *Soil Dyn*. *Earthq*. *Eng*., **105**, 11-21. https://doi.org/10.1016/j.soildyn.2017.11.016.

CC